Soil & Tillage Research 245 (2025) 106320

Contents lists available at ScienceDirect

Soil & Tillage Research

journal homepage: www.elsevier.com/locate/still

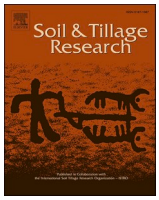

Biochar addition enhances silt loam soil resistance to rill flow: A study based on three years of field monitoring data on China's Loess Plateau

Yuanyuan Li [a], Yuan Yuan [a], Jiaqi Zhao [a], Jiayan Yang [b], Chuang Yan [c], Mingyi Yang [b,d], Bing Wang [b,d], Fengbao Zhang [b,d,*]

[a] School of Agricultural Sciences, Zhengzhou University, Zhengzhou 450001, China
[b] State Key Lab. of Soil Erosion and Dryland Farming on the Loess Plateau, Institute of Soil and Water Conservation Northwest A&F University, Yangling, Shaanxi 712100, China
[c] Institute of Geographical Sciences, Henan Academy of Sciences, Zhengzhou 450052, China
[d] Institute of Soil and Water Conservation, CAS and MWR, Yangling, Shaanxi 712100, China

ARTICLE INFO

Keywords:
Biochar amendment
Soil erosion resistance
Rill erodibility
Critical shear stress
Structural equation models
Loess Plateau

ABSTRACT

Biochar addition can change the physiochemical properties of soil, thus likely influencing soil's resistance to rill flow (reflected by rill erodibility (K_r, s m^{-1}) and critical shear stress (τ_c, Pa). However, the persistent time effects of biochar on K_r and τ_c have remained unexplored. This study aimed to assess the impact of biochar composed of apple branches on K_r and τ_c, and to investigate the relationships between K_r, τ_c and soil properties. The undisturbed soil core samples to a depth of 5 cm were collected from field plots that had received biochar at rates of 0, 1, 2.5, 4, 5.5, and 7 % (w/w) after 1, 2, and 3 years, respectively. The K_r and τ_c of these samples were evaluated through a flume experiment, with scouring soil samples under three flow discharges (e.g., 0.00025, 0.00045, and 0.00065 m^{-3} s^{-1}) and five slope gradients (e.g., 5.24, 8.75, 17.63, 26.79, and 40.40 %). The results revealed that the ranges of K_r and τ_c for no biochar treatments varied from 0.1947 to 0.2107 s m^{-1} and 1.6971–1.7314 Pa, with the averaged values of 0.2007 s m^{-1} and 1.7100 Pa, respectively. Compared with no biochar addition, the addition of 1–4 % biochar after 1–2 years generally resulted in a reduction in K_r ranging from 20 % to 59 %, while increasing τ_c by 2–4 %. Conversely, 5.5 and 7 % biochar addition increased K_r by 31 and 5 %, and reduced τ_c by 12 and 6 %. All biochar treatments after 3 years resulted in a 51 % reduction in K_r and a 5 % increase in τ_c relative to bare soil, showing an increasing trend with an increasing biochar addition rate. The fluctuations in K_r and τ_c could be elucidated by changes in cohesion (COH) and mean weight diameter of soil aggregates (MWD), with COH (total effect of −0.32 and 0.17, $P<0.01$) and MWD (total effect of −0.13 and 0.37, $P<0.01$) serving as reliable estimators of K_r and τ_c during the 1–2 years following biochar addition. After biochar addition for 3 years, total organic carbon (TOC) (total effect of −0.45 and 0.10, $P<0.01$) emerged as a significant factor influencing K_r and τ_c, making TOC a potential predictor of K_r and τ_c. The results demonstrate that biochar may be an effective measure for enhancing soil resistance to erosion on the Loess Plateau, especially when applied over the long term.

1. Introduction

Overland soil erosion by water can be divided into interrill, rill, and ephemeral gully erosions occurring on hillslopes (Gyssels et al., 2002; Shi et al., 2022a, 2022b). The Loess Plateau is situated in the arid and semi-arid regions of north-central China, covering an area of approximately 640,000 km^2. The dominant soil type in this region is loess, which is susceptible to erosion by wind and water, with gullies being the major landform types. The average annual precipitation ranges from 400 to 600 mm, primarily occurring as high-intensity storms between June and August (Tang et al., 2018). Rill erosion, defined as soil detachment, occurs within a narrow, erodible waterways, serving as a primary source and mechanism for sediment transportation in hillslope erosion processes (Niu, et al., 2020). On China's Loess Plateau, rill erosion constitutes about 70 % of the total erosion in upland areas (He et al., 2006). Rill erodibility (K_r) and critical shear stress (τ_c) reflect soil

* Corresponding author at: State Key Lab. of Soil Erosion and Dryland Farming on the Loess Plateau, Institute of Soil and Water Conservation Northwest A&F University, Yangling, Shaanxi 712100, China.
E-mail address: fbzhang@nwsuaf.edu.cn (F. Zhang).

https://doi.org/10.1016/j.still.2024.106320
Received 10 June 2024; Received in revised form 30 September 2024; Accepted 1 October 2024
Available online 11 October 2024

resistance to detachment by overland flow. The K_r is defined as the increase in soil detachment capacity caused by per unit increase in shear stress of flowing water (Meinen and Robinson, 2021). The τ_c refers to the minimum shear stress exerted by flowing water that is required to initiate the detachment and movement of soil particles (Al-Madhhachi et al., 2013). Thus, K_r and τ_c are important parameters for estimating the rill erosion rate in most process-based erosion models. The alteration of K_r and τ_c are notably influenced by essential soil physicochemical properties, such as soil organic carbon, soil cohesion, soil aggregates, and penetration resistance (Wang and Zhang, 2021). K_r and τ_c can be predicted using soil properties based on the regression equations from the WEPP (Water Erosion Prediction Project) model (Hao et al., 2021).

Biochar, also referred to as bio-char and agrichar, is a carbon-rich product produced through the thermochemical pyrolysis of biomass materials, such as livestock manure, sewage sludge or crop residue. Most studies investigating the effects of biochar addition have shown that it promotes soil aggregation and augments soil surface roughness, thereby enhancing soil cohesion and resistance to penetration (Kang et al., 2022; Situ et al., 2022). However, biochar addition has also been found to decrease soil bulk density and elevate soil porosity, thereby increasing soil looseness (Guo et al., 2022; Liang et al., 2021; Zhang et al., 2021). Moreover, biochar frequently exhibits high pH (Gao et al., 2021), which has the potential to elevate soil pH, leading to increased dispersibility of clay as a result of repulsive forces between clay minerals. Busscher et al. (2010) showed that the addition of biochar derived from pecan shells to loamy sand caused a great reduction in soil aggregation. Variations in soil properties caused by biochar addition have implications its use in controlling soil erosion.

The effects of biochar on soil erosion have been extensively investigated, however, findings have been inconsistent. Most studies have found that biochar addition could greatly reduce both runoff and sediment transport by improving the physicochemical properties of soil (Gholamahmadi et al., 2023; Li et al., 2024; Maisyarah et al., 2023; Shi et al., 2022a, 2022b; Vahidi et al., 2022). Conversely, other studies have reported that biochar has the opposite effect on soil erosion. Yin et al. (2024) observed that a biochar addition of 15–60 t ha^{-1} increased the accumulation of SOC, but elevated the surface runoff rate and surface soil loss on karst slopes. Zhang et al. (2019) cautioned against the addition of high biochar rates (8 %) on the slope soils, as it reduced runoff but may exacerbate soil erosion due to great improvements in soil chemical quality. In the Loess Plateau of China, Li et al. (2019) observed that the application of biochar at a rate of 7 % reduced saturated hydraulic conductivity (K_{sat}), thus leading to an increase in soil erosion, while lower application rates elevated water-stable soil aggregates and K_{sat}, resulted in a reduction of soil loss. Contrastingly, Ahmadi et al. (2020) noted that the incorporation of rice husk biochar at 1 kg m^{-2} resulted in elevated soil erosion, while higher rates (2 and 3 kg m^{-2}) reduced soil erosion in loamy soil within a semi-regional area. Additionally, Huang et al. (2021) demonstrated that wood biochar and pig manure biochar reduced soil water retention, but enhanced runoff and soil erosion in granite residual soil.

The inconsistent effects of biochar on soil erosion observed in previous studies indicate an uncertain variation in erodibility, the measure of soil erosion potential. However, research evaluating the impact of biochar addition on soil erodibility specifically is limited. Zhang et al. (2019) documented that 5 % and 8 % biochar additions led to a reduction of interrill erodibility, while the opposite result was observed for 2 % biochar addition. Parhizkar et al. (2023) recently explored the effect of rice husk biochar on K_r in deforested hillslopes of Northern Iran, and found that biochar addition significantly improved soil water-stable aggregate, and effectively reduced K_r. These contrasting results suggest that the influence of biochar on interrill and rill erodibility may differ, confirming the inconsistent effect on overall soil erosion, which is determined by soil erodibility, τ_c, flow shear stress and transportation.

Thus, exploring the variation of soil K_r and τ_c is a prerequisite, and will clarify the reason for the inconsistent effects of biochar on soil erosion. However, whether long-term biochar addition to soil affected K_r and τ_c has not been well investigated and documented. Few studies have

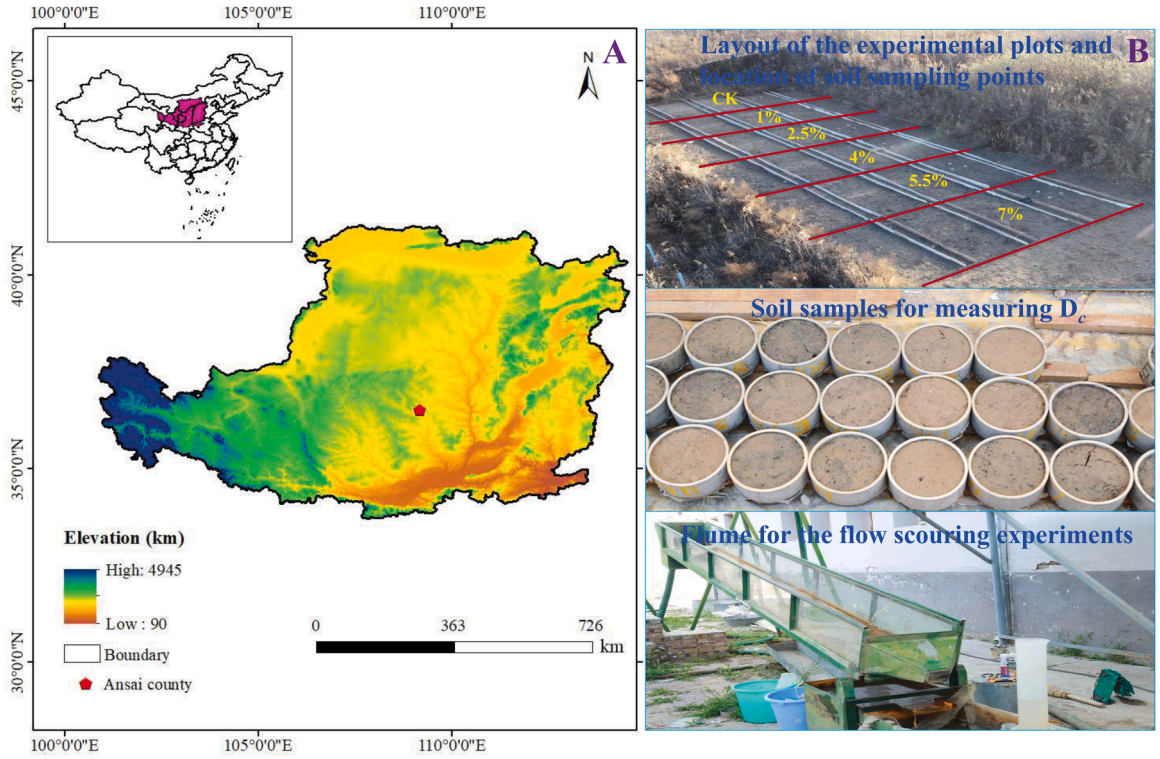

Fig. 1. Location of the study area, (A) plots, (B) soil sampling points and (C) equipment.

Table 1
Selected physicochemical properties of experimental materials.

Sample	Particle size distribution (%)			BD	pH	SSA	CEC	TOC	TN	TP	TK
	<0.002 mm	0.002–0.05 mm	0.05–2 mm	g·cm^{-3}		m^2 g^{-1}	cmol kg^{-1}	g kg^{-1}			
Loess	9.84	63.62	26.54	1.18	8.72	0.59	NA	4.44	0.41	0.53	19.56
Biochar	90.21	7.89	1.90	NA	8.96	9.96	2.22	331.50	3.31	0.95	7.35

BD, bulk density; SSA, specific surface area; CEC, cation exchange capacity; TOC, total organic carbon; TN, total nitrogen; TP, total phosphorus; TK, total potassium. NA= not applicable.

used a non-erodible bed inset with a small soil sample for measuring K_r and τ_c. This design enables accurate measurement by preventing sediment deposition, allowing for the assessment of the maximum detachment rate of soil samples by clean water. It effectively eliminates the sediment feedback effect caused by increased sediment load in rill flow and the deposition of soil particles. The flume experiment was conducted using the non-erodible bed with a small inset soil sample design in this study. This study was conducted (1) to investigate the response of K_r and τ_c to different rates and durations of biochar addition, (2) to explore the dominant factors influencing the temporal variation in K_r and τ_c on the Loess Plateau of China, (3) to establish an equation to estimate soil resistance for the Loess region using affecting factors under biochar addition. Ultimately, results from this study will offer a scientific assessment to ascertain the viability of biochar as an option for ameliorating degraded soil on cultivated slopes. Furthermore, this study will contribute to a better understanding of the potential benefits and limitations of biochar addition in soil erosion management and soil restoration efforts.

2. Materials and methods

2.1. Study location

The study was conducted at the Ansai Field Station of the Institute of Soil and Water Conservation, Chinese Academy of Sciences, located in the northern part of the Loess Plateau in China (109°18 ' 51 " E, 36°51 ' 15 " N; Fig. 1A). The region features a semi-arid continental climate, with an average annual precipitation of 505 mm. More than 70 % of this precipitation occurs from June to September, typically as short and intense rainstorms. The average daily temperature ranges from −16.15°C to 16.63 °C, with a mean of 9.26 °C. The soil in the study area primarily originates from wind-deposited loess parent material and is classified as a typical silt loam (26.5 % sand, 63.6 % silt, 9.8 % clay) according to the USDA classification. The soil exhibits a low level of total organic carbon at 4.44 g kg^{-1} and a bulk density of 1.18 g·cm^{-3}, characteristics commonly associated with structurally poor and loose soils. Here, as in other countries and locales, human activities exacerbate soil erosion and degradation (Delgado, 2018; Ebabu et al., 2023; Ferreira

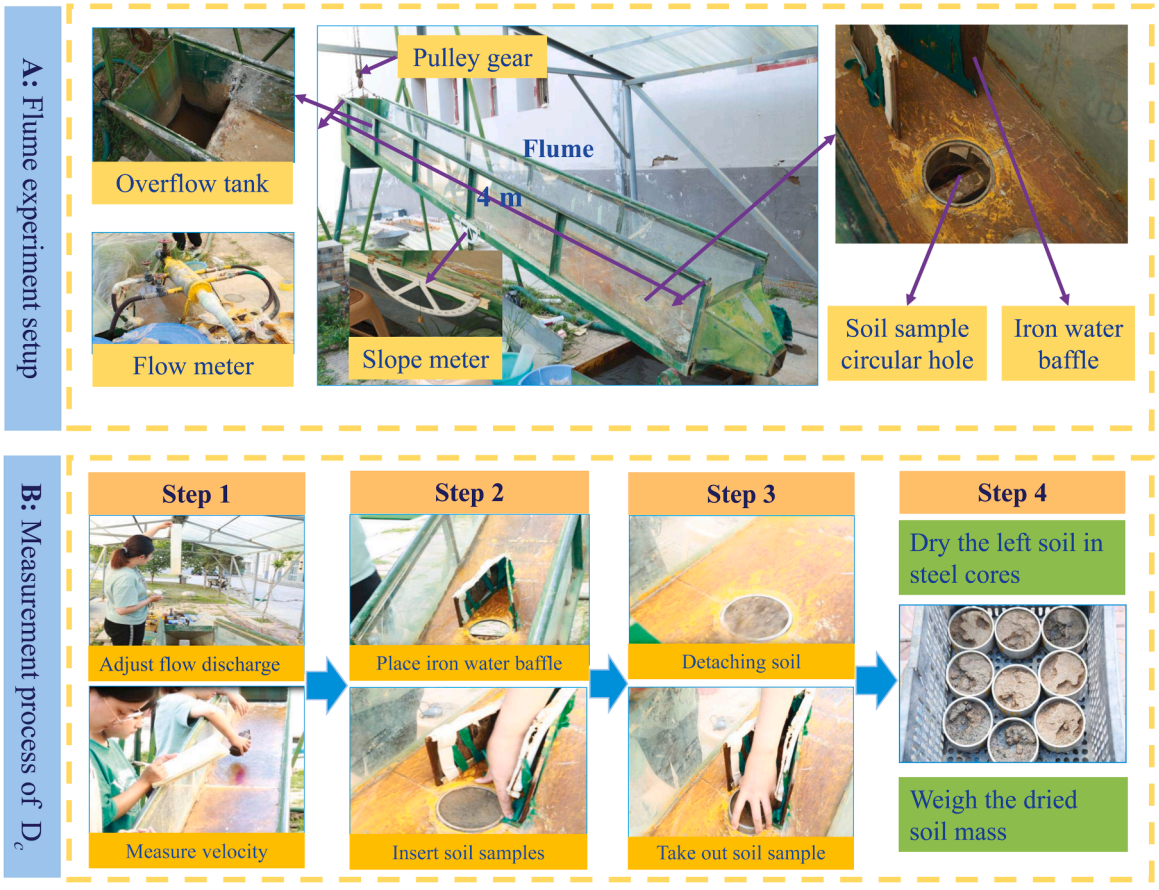

Fig. 2. The flume experiment setup (A) and measurement process of D_c (B) in this study.

et al., 2022; Parhizkar et al., 2021). The combination of intense rainstorms, erodible soil, and human activities often leads to severe soil erosion and degradation in this area.

2.2. Biochar description

The biochar, sourced from the Shaanxi Yixing Technology Co., Ltd., Xi'an, China, was produced by pyrolyzing apple branches obtained from local orchards known for large-scale apple production. Pyrolysis was conducted at around 550 °C, and the resulting biochar, after drying, was transported to the study area for application in experimental plots and to the lab for basic properties analysis. The biochar pH was determined through electrochemical analysis at a biochar: deionized water ratio of 1:15 (w/v). Total organic carbon (TOC) and total nitrogen (TN) were measured using an Elementar (German Element, GRE). The specific surface area of biochar was obtained using N_2 absorption at 77 K using a V-Sorb 2800 P SSA, and the CEC was assessed using the ammonium acetate exchange method. Selected physicochemical of both soil and biochar are presented in Table 1.

2.3. Experimental plot design

The experimental field (about 25 m×6 m) was a flat terraced area situated on the top of a plateau with an elevation of about 1268 m. It had been left abandoned for several years. Before all plots were set, all vegetation and roots were removed through ploughing to a depth of 20 cm. The experiment plot design was a randomized complete block with six different biochar treatments and three replications. The resulting experiment site was a field divided into 18 plots, each measuring 1.5 m in width and 4 m in length, with rows separated by a 0.3-m alleyway (Fig. 1B). In August 2017, the biochar derived from clipped apple branches was mixed with the top 20 cm of soil in each plot with six rates of 0, 1 %, 2.5 %, 4 %, 5.5 %, 7 %. These rates were selected based on the range of biochar application rates (0.25 %~10 %) commonly used in previous studies (Abrol et al., 2016; Zeng et al., 2014), and they were also similar to those used in a simulated experiment by Li et al. (2019). After the biochar was mixed, each plot was ploughed again to a depth of 20 cm to follow local farming practices for a uniform mixture. Biochar was added once in 2017, and wasn't applied again in 2018, 2019 or 2020. No crops were planted in the experimental plots during the study. After ploughing all plots to a depth of 20 cm every year in May from 2018 to 2020, any weeds that appeared were periodically removed without disturbing the soil surface.

2.4. Soil sampling for measuring D_c

After the addition of biochar in 2017, intact soil samples from a depth of 0–5-cm were collected from each soil plot once annually from 2018 to 2020. Sampling events occurred in August every year, corresponding to one, two, and three years after the biochar addition. Circular steel rings with a 10.0 cm diameter and 5.0 cm depth were used to collect the soil carefully while minimizing disturbances to the surrounding area. In order to obtain soil sample uniformly in the whole plots, avoid sampling bias and improve data quality, soil samples were randomly collected from each plot in an "S"-shaped pattern. Once the top rim of each ring was flush with the ground surface, the rings were carefully excavated, lifted, and turned over, taking care to remove any excess soil from the bottom of the rim without disturbing the soil core. To prevent disturbance during transport, the tops and bottoms of the steel rings were cushioned with cotton cloth, covered with a lid, and sealed with plastic wrap. Three soil samples were collected at each plot as replicates. For each soil sample, soil moisture and dry soil weight were measured. Disturbed soil samples were also collected from the same depth and location as the ring sample for soil moisture measurement. Following soil sample collection, a 12-hour saturation process was performed in a water-filled container, with the water level maintained below 1 cm from the top of the soil surface. Next, the saturated soil samples were drained for 12 hours to achieve consistent soil water content (Fig. 1B).

The experiment involved three different flow discharges (0.00025, 0.00045, and 0.00065 m^{-3} s^{-1}) and five slope gradients (5.24 %, 8.75 %, 17.63 %, 26.79 %, and 40.40 %). The range of five slope gradients also reflects those adopted in the "Grain for Green" project, which provides the guidance that arable land on steep slopes over 25° should be converted to forest or grazing land (Zhang et al., 2023). The experiment further incorporated six biochar treatments at varying levels: 0, 1 %, 2.5 %, 4 %, 5.5 %, 7 %. Each combination of flow discharge, slope gradient, and biochar treatment was tested in triplicate. Consequently, a total of 270 samples were collected each year from the six plots treated with biochar to measure D_c.

2.5. Experimental devices

A rectangular flume measuring 4 m in length, 0.35 m in width, and 0.2 m in depth was used to assess D_c (Fig. 2B). This is identical to flumes used in other studies (Wang et al., 2018; Zhang et al., 2020). The size of the flume was based on a critical rill length of 4 m and rill depths ranging from 0.05 to 0.15 m on the Loess Plateau (Lei et al., 2002). To

Table 2
Relationship between K_r and τ under different rates and durations of biochar addition.

Year	BC addition rate	Equation of regression	K_r	τ_c	R^2	*P*	RMSE	MAE	n
2018	CK	D_c=0.1981(τ−1.7032)	0.1981	1.7032	0.8173	<0.01	0.1155	0.0941	15
	1 %	D_c=0.1585(τ−1.7338)	0.1585	1.7338	0.8148	<0.01	0.0931	0.0754	15
	2.5 %	D_c=0.1227(τ−1.7561)	0.1227	1.7561	0.8672	<0.01	0.0605	0.0501	15
	4 %	D_c=0.0838(τ−1.7792)	0.0838	1.7792	0.8719	<0.01	0.0430	0.0380	15
	5.5 %	D_c=0.2717(τ−1.4921)	0.2717	1.4921	0.8875	<0.01	0.1193	0.0928	15
	7 %	D_c=0.2264(τ−1.5720)	0.2264	1.5720	0.8983	<0.01	0.0939	0.0829	15
2019	CK	D_c=0.1971(τ−1.7078)	0.1971	1.7078	0.8082	<0.01	0.1344	0.1074	15
	1 %	D_c=0.1569(τ−1.7390)	0.1569	1.7390	0.7996	<0.01	0.0857	0.0733	15
	2.5 %	D_c=0.1219(τ−1.7416)	0.1219	1.7416	0.8306	<0.01	0.0610	0.0508	15
	4 %	D_c=0.0782(τ−1.7650)	0.0782	1.7650	0.8285	<0.01	0.0411	0.0355	15
	5.5 %	D_c=0.2463(τ−1.5043)	0.2463	1.5043	0.8856	<0.01	0.2179	0.1802	15
	7 %	D_c=0.1884(τ−1.6428)	0.1884	1.6428	0.8499	<0.01	0.3082	0.2456	15
2020	CK	D_c=0.1894(τ−1.7187)	0.1894	1.7187	0.7796	<0.01	0.0352	0.1047	15
	1 %	D_c=0.1173(τ−1.7415)	0.1173	1.7415	0.8601	<0.01	0.0151	0.0468	15
	2.5 %	D_c=0.1096(τ−1.7651)	0.1096	1.7651	0.8407	<0.01	0.0154	0.0497	15
	4 %	D_c=0.0663(τ−1.7897)	0.0663	1.7897	0.8197	<0.01	0.0107	0.0354	15
	5.5 %	D_c=0.1591(τ−1.7291)	0.1591	1.7291	0.7660	<0.01	0.0280	0.0865	15
	7 %	D_c=0.0108(τ−2.003)	0.0108	2.003	0.5637	<0.01	0.0045	0.0113	15

BC, biochar; K_r, rill erodibility (s m^{-1}); τ_c, critical shear stress (Pa); R^2, determination coefficient; *P*, significance level; RMSE, root mean square error; MAE, mean absolute error (%); n is sample size.

simulate a natural soil surface, soil from the experiment plots without biochar were passed through a 5 mm sieve, then glued evenly onto the flume bed, forming a consistent soil layer. The slope gradient of the flume could be manually adjusted within the slope range of 1°~25° using a pulley gear located at the top of the flume, with precise measurements obtained from a slope meter (Fig. 2A). Flow discharge was controlled with a flow meter and calibrated using a graduated cylinder which collected water flow within a unit time from the flume before D_c measurement. A soil sample circular hole with a diameter of 10.1 cm, just large enough to hold the soil sample rings, was situated 0.6 m from the flume's end outlet (Fig. 2A). An iron water baffle was positioned in front of the circular hole to regulate water flow and manage the soil detachment process caused by the flow from the flume (Fig. 2A).

2.6. Measurement of hydrodynamic parameters

Before detaching the soil samples, the hydrodynamic parameters of the flume flow were measured. After achieving steady water flow for each slope and flow discharge from the flume, the surface velocity of the flume flow was determined using the $KMnO_4$ method. This involved recording the time required for water with $KMnO_4$ to traverse a distance of 2 m above the front end of the circular hole containing the soil sample ring (Wang et al., 2018). Surface flow velocity was measured at six points, evenly spaced from left to right across the width of the flume. Each point was measured three times resulting in 18 values, which were then averaged to calculate the mean surface flow velocity (v_m, m s^{-1}) (Fig. 2B). During this measurement, the temperature of the flume flow was monitored using a mercurial thermometer to estimate the viscosity coefficient (V, m^2 s^{-1}). Subsequently, the Reynolds number (Re) (Foster, 1982) was calculated based on Eq. (1):

$$\mathrm{Re} = \frac{\mathrm{R}vm}{\mathrm{V}} \tag{1}$$

Where R represents hydraulic radius (m); V denotes viscosity coefficient of the flume flow (m^2 s^{-1}); v_m is the mean surface flow velocity (v_m, m s^{-1}).

The pattern of the flume flow was classified as laminar flow (Re<2000), transitional flow (2000<Re<4000), or turbulent flow (Re>4000). The average velocity of the flume flow (v, m s^{-1}) for each combination of one flow discharge and one slope was obtained by multiplying the mean surface flow velocity (v_m) by coefficients of 0.6 (laminar flow), 0.7 (transitional flow) and 0.8 (turbulent flow), respectively, based on the pattern of the flume flow (Cao et al., 2011; Luk and Merz, 1992) (Table 2). The flow depth (h, m) (Nearing et al., 1991; Liu et al., 2024) was calculated as follows:

$$\mathrm{h} = \frac{\mathrm{Q}}{v\mathrm{B}} \tag{2}$$

Here, Q refers to the flow discharge (m^3 s^{-1}), v is the mean flow velocity (m s^{-1}), B is the width of flume (B=0.35 m).

Subsequently, shear stress (τ, Pa) (Cochrane and Flanagan, 1997) was computed based on Eq. (3):

$$\tau = \rho \mathrm{ghS} \tag{3}$$

Where ρ, g, and S represent the water density (ρ=1 kg m^{-3}), gravitational acceleration (g=9.8 m s^{-2}), and sine value of slope gradients. Fifteen shear stresses ranging from 1.05 to 5.35 *Pa* were obtained by combining three flow discharges (250, 450, and 650 ml s^{-1}) with five slope gradients (5.24 %, 8.75 %, 17.63 %, 26.79 %, and 40.40 %).

2.7. Measurement of D_c by overland flow, and calculation of K_r and τ_c

Soil detachment capacity (D_c) was measured through a series of flow scouring experiments carried out each year using a flume (Fig. 2B), following the experimental process described by Zhang et al. (2003). The measurement process for D_c involved the following steps:

Step 1: Set the desired slopes and adjusted the flow discharge using a flow meter calibrated with a graduated cylinder in the flume. Measured the surface velocity of flume flow using the $KMnO_4$ method.

Step 2: Placed an iron water baffle in front of the circular hole to halt water flow in the flume, then inserted a soil sample ring into the soil sample circular hole located before the flume's bottom.

Step 3: Removed the iron water baffle to allow the water flow to detach soil from the soil sample ring. Stopped the detachment once the scoured soil depth in the soil sample ring reached approximately 2 cm because when the scoured soil depth is less than 2 cm, the impact of the ring's sidewall on D_c is the minimum (Zhang, 2002). Meanwhile, recorded the duration of the flow scouring process with a chronograph.

Step 4: Dried the wet soil remaining in the soil sample ring at 105 °C in an oven for 24 hours, then weighed the dried soil mass using an electronic balance to determine the final weight of the dry soil left in the soil sample ring after the flow scouring experiments.

D_c was calculated using Eq. (4):

$$\mathrm{Dc} = \frac{\mathrm{Mo} - \mathrm{Mf}}{\mathrm{a} * \mathrm{t}} \tag{4}$$

Table 3
Basic variation of experimental soil properties with biochar addition from 2018 to 2020.

Year	BCR	COH	LSD	MWD	LSD	BD	LSD	TC	LSD	TOC	LSD
	%	*Kpa*		mm		g m^{-3}		g kg^{-1}		g kg^{-1}	
2018	CK	12.88b		0.91d	0.06	1.18a		18.71d		4.44 f	
	1	18.27a		1.02c		1.11ab		28.03c		6.26e	
	2.5	18.86a		1.19b		1.07abc		29.54c		20.00d	
	4	19.35a	1.29	1.28a		1.06bc	0.12	53.22b	0.24	37.86a	0.91
	5.5	10.57c		0.70e		1.01bc		52.67b		29.34c	
	7	11.33 cd		0.89d		0.97c		76.81a		34.69b	
2019	CK	12.59d	0.71	0.92c		1.15a		18.3d		5.27 f	
	1	19.53b		1.18b		1.08ab		27.6c		11.36e	
	2.5	17.35c		1.16b		1.05ab		29.1c		12.49d	
	4	22.81a		1.29a	0.07	1.04ab	0.14	52.8b	0.35	22.33c	0.98
	5.5	11.52e		0.56d		1.00b		52.2b		27.22b	
	7	12.26d		0.88c		0.99b		76.4a		35.14a	
2020	CK	13.49e		0.91d		1.23a		17.70 f		7.40 f	
	1	18.49c		1.14c		1.17ab		24.41e		12.02e	
	2.5	18.78c		1.18c		1.12b		31.73d		15.97d	
	4	24.76b	0.62	1.33b	0.06	1.10bc	0.10	44.50c	0.30	19.56c	1.00
	5.5	17.67d		1.16c		1.08bc		57.92b		25.40b	
	7	32.96a		2.03a		1.01c		61.30a		28.53a	

BC, biochar; COH, cohesion (*Pa*); MWD, mean weight diameter of soil aggregate (mm); BD, bulk density (g cm^{-3}); TC, total carbon (g kg^{-1}); TOC, total organic carbon (g kg^{-1}). Values followed by different lower letters within a column are statistically significant at P<0.05 based on LSD test between different rates.

Table 4
Variation of rill erodibility (K_r, s m^{-1}) and critical shear stress (τ_c, Pa) with biochar addition from 2018 to 2020.

Year	BC addition rate	K_r	τ_c
	%	s m^{-1}	Pa
2018	CK	0.1981±0.0033b	1.7032±0.0024ab
	1	0.1585±0.0069c	1.7338±0.0766a
	2.5	0.1227±0.0267d	1.7561±0.1438a
	4	0.0838±0.0059e	1.7792±0.0496a
	5.5	0.2717±0.0504a	1.4921±0.0228c
	7	0.2264±0.0134b	1.5720±0.0261bc
Contrast		*Pr>F*	
	Biochar *vs* Control	0.004	<0.001
2019	CK	0.1971±0.0022b	1.7078±0.0044ab
	1	0.1569±0.0138c	1.7390±0.0335a
	2.5	0.1219±0.0342 cd	1.7416±0.1891a
	4	0.0782±0.0078d	1.7650±0.0367a
	5.5	0.2463±0.0296a	1.5043±0.1190c
	7	0.1884±0.0232b	1.6428±0.0431b
Contrast		*Pr>F*	
		Pr>F	
		Pr>F	
	Biochar *vs* Control	<0.001	<0.001
2020	CK	0.1894±0.0055a	1.7187±0.0151b
	1	0.1173±0.0060c	1.7415±0.0396b
	2.5	0.1096±0.0248c	1.7651±0.0123b
	4	0.0663±0.0033d	1.7897±0.0569b
	5.5	0.1591±0.0074b	1.7291±0.0661b
	7	0.0108±0.0007e	2.0030±0.0188a
Contrast		*Pr>F*	
Pr>F			
	Biochar vs Control	<0.001	<0.001
	Duration main effect of biochar addition		
	2018	0.1726±0.0766 A	1.6806±0.1513 A
	2019	0.1609±0.0624 A	1.6785±0.1421 A
	2020	0.0926±0.0521B	1.7970±0.4566B

Values followed by different lowercase letters within a column are statistically significant at $P<0.05$ based on an LSD test between different rates under the same year. Different capital letters within a column are statistically significant at $P<0.05$ based on an LSD test between biochar addition durations averaged addition rates.

Table 5
Analysis of variance of significance and contribution rate of the interaction of variables affecting soil K_r and τ_c.

Indicators	Source	*df*	Mean squares	*F* value	Sig.	Contribution ratio (%)
K_r	D	2	0.022	1343.068	0.000	**19**
	R	5	0.027	1617.136	0.000	**56**
	D*R	10	0.006	368.698	0.000	25
	Error	36	0.002			0.4
τ_c	D	2	0.001	4.248	0.022	0.4
	R	5	0.050	172.545	0.000	**49**
	D*R	10	0.026	88.733	0.000	**48**
	Error	36	0.000			3

K_r, rill erodibility (s m^{-1}); τ_c, critical shear stress (Pa); D, duration of biochar application (year); R, rate of biochar application (%); *df*, degree of freedom; Sig., significance.

Where D_c represents the soil detachment capacity by flume flow (kg m^{-2} s^{-1}); M_o is the weight of the soil sample dried before the flow scouring experiments (kg); M_f represents the mass of the soil sample (kg) left in the soil sample ring after the flow scouring experiments; a denotes the cross-sectional area of the steel ring (m^2), and t indicates the period tested (s).

The soil erosion resistance parameters K_r and τ_c are key metrics in evaluating soil susceptibility to rill erosion. K_r is the rate at which D_c increases with each unit increase in flow shear stress, and τ_c represents a threshold value, beyond which there is a significant increase in D_c for each unit increase in shear stress. In the Water Erosion Prediction Project (WEPP) model (Flanagan and Nearing, 1995), K_r and τ_c were estimated based on the measured D_c and τ using Eq. (5):

$$Dc = Kr(\tau - \tau c) \quad (5)$$

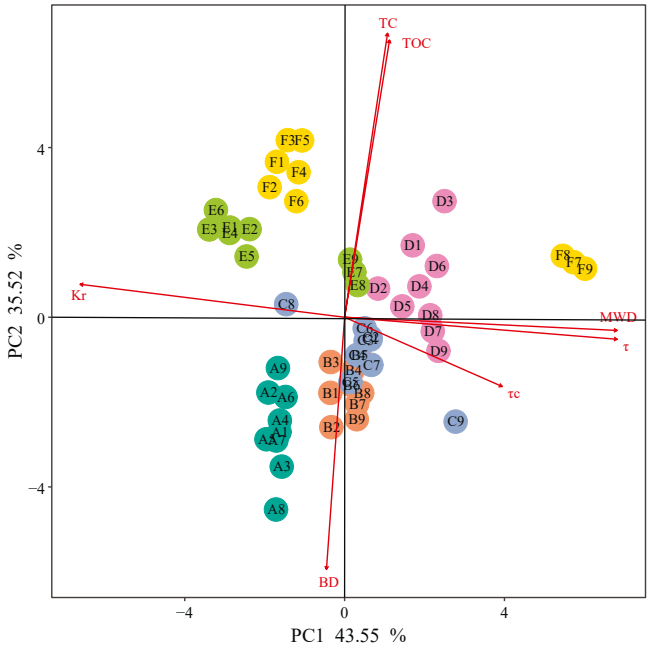

Fig. 3. Principal component analysis of rill erodibility (K_r), critical shear stress (τ_c) and soil physicochemical parameters in different biochar addition rates and durations (n=9). COH, cohesion (*Pa*); MWD, mean weight diameter of soil aggregate (mm); BD, bulk density (g cm^{-3}); TC, total carbon (g kg^{-1}); TOC, total organic carbon (g kg^{-1}).

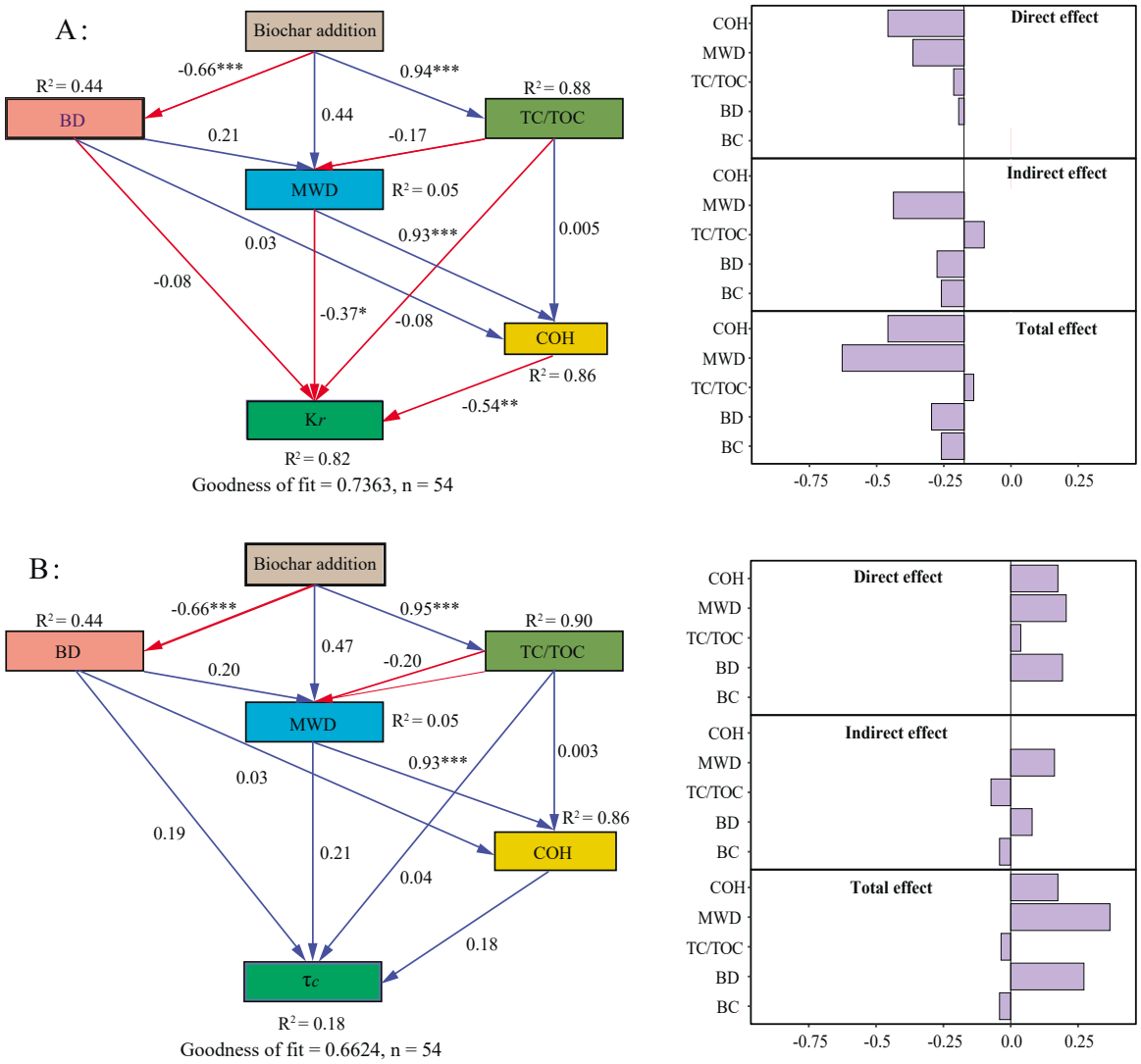

Fig. 4. Structural equation models (SEMs) illustrating the effects of biochar addition on soil rill erodibility (K_r) and critical shear stress (τ_c). Standardized path coefficients are represented by red (negative) and blue (positive) arrows. Numbers adjacent to arrows indicate effect sizes. $^*P<0.05$, $^{**}P<0.01$. COH, cohesion (*Pa*); MWD, mean weight diameter of soil aggregate (mm); BD, bulk density (g cm^{-3}); TC, total carbon (g kg^{-1}); TOC, total organic carbon (g kg^{-1}).

Where K_r represents rill erodibility (s m^{-1}), and τ_c denotes the critical shear stress (Pa).

A lower K_r and higher τ_c indicate greater soil erosion resistance. In this equation, D_c is considered to increase linearly with an increase in τ. In the scatter plot with τ on the x-axis and D_c on the y-axis, the slope of fitted line is K_r, while the x-intercept corresponds to τ_c. Thus, the regression-derived values of K_r and τ_c were obtained for all biochar treatments at each sampling time (Table 2).

2.8. Soil properties measurement

Soil cohesion (COH), mean weight diameter of soil water-stable aggregates (MWD), bulk density (BD), total carbon (TC), and total organic carbon (TOC) were measured for the topsoil of all plots at the time of each sampling to determine the variations of K_r and τ_c each year. BD of the 0–5 cm soil layer was obtained for six duplicates using steel rings (5 cm diameter×5 cm height) via the oven-dried method. A Eijkelkamp pocket vane tester was used to determine the COH, with six readings taken (Shen et al., 2021a, 2021b). The wet-sieving method was employed to measure the soil water-stable aggregate in triplicate (An et al., 2013), then MWD was calculated based on the distribution of soil water stable aggregate (Klute et al., 1986). TC and TOC were obtained using a Vario EL cube elemental analyzer from German Element (German Element, GRE), and the potassium dichromate colorimetric method was used in triplicate. The average COH, MWD, BD, TC, and TOC for each biochar treatment are presented in Table 3.

2.9. Statistical analysis

One-way ANOVA determines if the independent variable has a significant effect on the dependent variable, and Least Significant Difference (LSD) is a post-hoc test used after ANOVA to determine which specific groups are significantly different from each other. Thus, One-way ANOVA was conducted, followed by LSD ($P<0.05$) to compare variations in soil properties, K_r and τ_c with different rates and durations of biochar addition. Two-way ANOVA examines both the individual effects of each factor on the dependent variable and any interaction effects between the two factors, and was used to determine the interaction effects between rates and durations of biochar addition with LSD ($P<0.05$). Additionally, the contribution ratio (CR) of the biochar addition rate and duration to the observed variations in K_r and τ_c was calculated using Eq. (6) (Sadeghi et al., 2012):

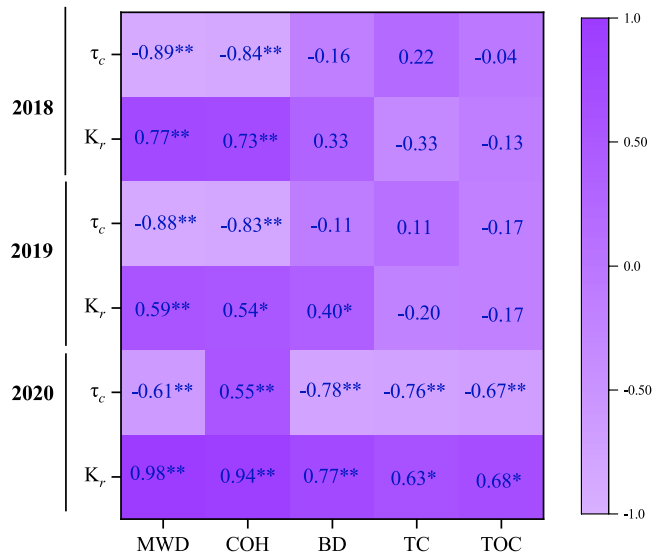

Fig. 5. Pearson correlation coefficient matrix between rill erodibility (K_r), critical flow shear stress (τ_c) and soil properties under different biochar application durations. *$P<0.05$, **$P<0.01$. COH, cohesion (*Pa*); MWD, mean weight diameter of soil aggregate (mm); BD, bulk density (g cm^{-3}); TC, total carbon (g kg^{-1}); TOC, total organic carbon (g kg^{-1}).

$$CR = \frac{SSF - (Df * VEr)}{SST} \times 100 \quad (6)$$

Where SS_T stands for total sum of squares, which represents the total variation in the dependent variable. SS_F refers to factorial sum of squares, which represents the variation in the dependent variable that is explained by the independent variables (in this case, biochar addition rate and duration). V_{Er} represents the variance of error, which is the unexplained variation in the dependent variable. Finally, D_f refers to degrees of freedom, which is a measure of the amount of information available to estimate statistical parameters.

Redundancy analysis (RDA) is used to investigate the relationships between two sets of variables: explanatory variables (e.g., environmental factors) and response variables (e.g., species data). The "vegan" package in R software (v. 4.0.2) was used for RDA, which identified correlations between sample distributions, K_r, τ_c, and soil properties. Environmental factors were selected using variance expansion analysis to eliminate collinearity for RDA. Partial Least Squares Path Modeling (PLS-PM) is a technique used in structural equation modeling (SEM) to analyze complex causal relationships among latent and observed variables. In this study, PLS-PM was employed to identify possible pathways for how variables control K_r and τ_c with the addition of biochar. The "innerplot" function in the "plspm" package was used to construct the models.

Simple regressions were used to quantify the relationships between D_c and τ, and determine the K_r and τ_c. Non-linear regression equations were utilized to comprehensively analyze the relationships between K_r, τ_c, and soil properties. To assess the fitness of the regression equations, coefficient of determination (R^2) was calculated. The modelling dataset used in this study was the same as the one used in previous studies (Liu et al., 2020; Shen et al., 2021a, 2021b; Wang et al., 2018). All statistical analyses were conducted using the R software package (v.4.0.2).

3. Results

In this study, applying biochar, regardless of the rates and duration of addition, generally weakened soil K_r while it enhanced τ_c. The K_r and τ_c for the control ranged from 0.1947 to 0.2107 s m^{-1} and 1.6971–1.7314 Pa, respectively, with a mean of 0.2007 s m^{-1} and 1.7100 Pa. In contrast, the K_r and τ_c for soils with biochar incorporation ranged from 0.0108 to 0.3334 s m^{-1} and 0.5700–2.9602 Pa, with a mean of 0.1412 s m^{-1} and 1.7216 Pa (Table 4). On average, across the

Table 6
Equations for modeling soil resistance (K_r and τ_c) from 2018 to 2020 under biochar addition (n=45).

Year	Equations	Number	R^2	*P*
2018	$K_r=e^{-0.699}MWD^{-1.603}COH^{-0.430}$	(7)	0.686	<0.01
	$\tau_c=e^{0.581}MWD^{0.327}COH^{-0.011}$	(8)	0.683	<0.01
2019	$K_r=e^{0.576}MWD^{-0.551}COH^{-0.776}$	(9)	0.669	<0.01
	$\tau_c=e^{0.606}MWD^{0.109}COH^{0.057}$	(10)	0.561	<0.01
2020	$K_r=e^{-3.052}MWD^{-4.572}COH^{0.017}TOC^{-0.555}$	(11)	0.931	<0.01
	$\tau_c= e^{-0.531}MWD^{-0.205}COH^{0.012}TOC^{-0.102}$	(12)	0.728	<0.01
2018–2020	$K_r=e^{1.742}MWD^{-1.029}COH^{-1.221}TOC^{-0.255}$	(13)	0.761	<0.01
	$\tau_c=e^{0.525}MWD^{0.224}$	(14)	0.605	<0.01

K_r, soil rill erodibility (s m^{-1}); τ_c, critical shear stress (Pa); COH, cohesion (*Pa*); MWD, mean weight diameter of soil aggregate (mm); TOC, total organic carbon (g kg^{-1}).

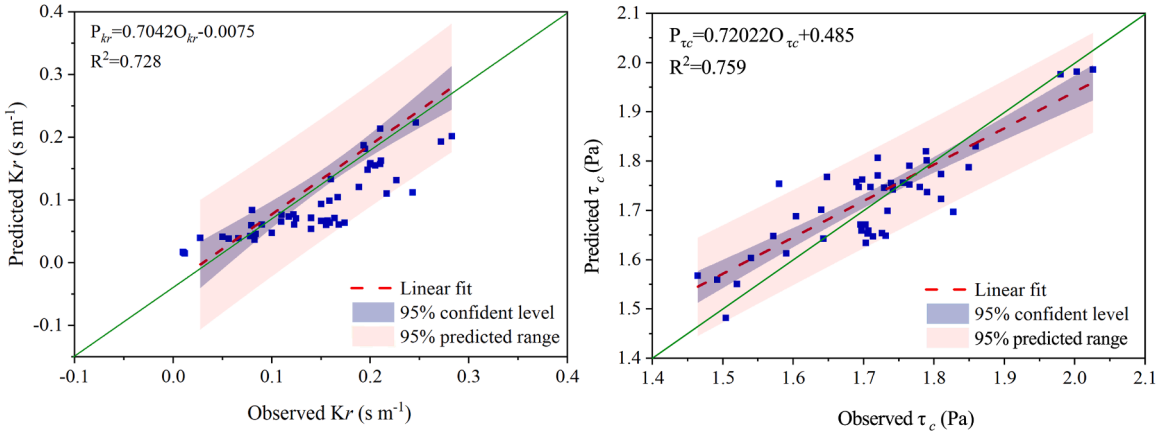

Fig. 6. Comparison of differences between observed and predicted rill erodibility (K_r) and critical flow shear stress (τ_c) using the established Eq. (13) and (14).

years of the study, there was a 30 % the reduction in K_r and 1 % increase in τ_c compared to the control. However, the effect of biochar on soil K_r and τ_c depended on the rate and duration of biochar addition (Table 5). The analysis of variance indicated that biochar addition rate, duration, and their interaction significantly affected K_r, with the biochar addition rate had contributed more to both K_r and τ_c (56 % and 49 %, respectively), followed by the interaction of biochar addition duration and rate, then biochar duration (Table 5).

3.1. Variations of soil resistance with biochar addition rate

The rate of biochar addition significantly affected both K_r and τ_c, with the rate of addition contributing more than the duration of addition and their interaction effects (Table 5). In 2018 and 2019, the mean K_r and τ_c without biochar were 0.1976 s m^{-1} and 1.7055 Pa, respectively. When biochar was applied at rates of 1 %, 2.5 %, and 4 %, K_r decreased to 0.1442, 0.1181, and 0.0761 s m^{-1} (Table 4), corresponding to reductions of 27 %, 40 % and 61 %, respectively. In contrast, τ_c increased by 2 %, 3 % and 4 %, with greater effect with higher biochar rates. Conversely, biochar addition at 5.5 % and 7 % increased K_r by 31 % and 5 % while reducing τ_c by 12 % and 6 %, compared to the control. In 2020, all biochar addition treatments (1 %, 2.5 %, 4 %, 5.5 % and 7 %) led to reductions in K_r of 38 %, 42 %, 65 %, 16 %, and 94 %, respectively, while τ_c increased by 1 %, 3 %, 4 %, 1 % and 17 % relative to bare soil.

3.2. Variations of soil resistance with biochar addition duration

The duration of biochar addition significantly influenced both K_r and τ_c (Table 5). In 2018, the range of K_r in biochar-treated soil was 0.0838–0.2717 s m^{-1}, with a mean of 0.1726 s m^{-1}. In 2019, K_r ranged from 0.0782 to 0.2463 s m^{-1}, with a mean of 0.1609. By 2020, K_r had a range of 0.0108–0.1894 s m^{-1}, with an average of 0.0926 s m^{-1} (Table 4). Relative to the control, biochar addition reduced K_r by 13 % in 2018, 20 % in 2019 and 94 % in 2020, indicating a positive correlation between the duration of biochar addition and the reduction in K_r. The most substantial decrease of K_r was observed in 2020 compared to the control. In contrast to K_r, biochar addition had no significant effect on τ_c in 2018 and 2019. However, τ_c increased by 17 % in 2020 compared to the control, indicating a significant impact (Table 4).

3.3. Correlation between soil properties and levels of resistance

The correlation matrix in Fig. 3 showed the interrelationships among the soil properties and levels of soil resistance. Generally, soil properties, such as mean weight diameter (MWD), cohesion (COH), total organic carbon (TOC) and bulk density (BD), exhibited a negative correlation with K_r but positive correlation with τ_c (Fig. 3). Notably, the most significant correlations were observed between K_r, τ_c and MWD and COH.

The changes of soil properties induced by biochar addition affected K_r and τ_c, however, the effect depended on the different soil properties (Fig. 4A). A conceptual model was developed to illustrate these relationships, demonstrating strong explanatory power for K_r (91 % of the variance explained, with a goodness of fit of 0.74). Biochar addition directly impacted BD, MWD, and TC, with standardized path coefficients of −0.66, 0.44, and 0.94, respectively. MWD had the most substantial effect on COH, with a standardized path coefficient of 0.93. Both MWD and COH showed significant negative effects on K_r, with standardized path coefficients of −0.37 and −0.54, respectively. The effects of MWD and COH on K_r were largely direct (-0.55 and −0.62) rather than indirect (-0.38 and −0.01) (Fig. 4A). In contrast, most soil properties had positive effects on τ_c, and the total effect of MWD, BD, and COH (0.32, 0.27, and 0.13) on τ_c was greater than that of TC (Fig. 4B). The conceptual model demonstrated good explanatory power for τ_c, explaining 83 % of the variance with a goodness of fit of 0.66, although these values were slightly lower than those observed for K_r.

Meanwhile, the correlation between soil resistance to soil erosion (K_r and τ_c) and soil properties also varied with biochar addition duration (Fig. 5). Pearson correlation analysis revealed significant effects between K_r, τ_c and MWD in both 2018 and 2019. However, a significant correlation between K_r, τ_c and soil carbon (TC and TOC) emerged only after three years of biochar addition in 2020 (Fig. 5).

3.4. Soil resistance estimation

Direct measurement of K_r and τ_c poses challenges under both field and laboratory conditions. Therefore, it is essential to estimate K_r and τ_c using easily measurable soil properties. The results indicated a close correlation between K_r, τ_c and soil properties, notably COH (0.73 and −0.84) and MWD (0.77 and −0.89), which were the key factors influencing K_r and τ_c in 2018 and 2019. Consequently, K_r and τ_c were estimated well by MWD and COH for the years of 2018 and 2019 with high R^2 values in the power regression Eq. (7) ~ (10) (Table 6, $P<0.01$), demonstrating a reliable approach for estimating these soil resistance metrics.

Over time, TOC started to significantly influence K_r and τ_c with high correlation coefficients of 0.68 and −0.67. Therefore, in 2020, TOC was included alongside COH and MWD to estimate K_r and τ_c, as illustrated by Eq. (11) and (12) (Table 6, $P<0.01$).

A comprehensive analysis of all the factors affecting K_r and τ_c from 2018 to 2020 indicated that K_r could be reliably estimated by MWD, COH and TOC, while τ_c could be estimated by MWD using a power function Eq. (13) and (14) (Table 6, $P<0.01$). The R^2 for Eq. (13) and (14) were 0.761 and 0.605, respectively, suggesting that both equations were effective in predicting K_r and τ_c during the three-year period of biochar addition. The predicted K_r and τ_c, derived from Eq. (13) and (14), align closely with the measured values from the flume experiment, falling along the 1:1 line. This observation underscores the high accuracy of both equations for predicting K_r and τ_c (Fig. 6). Therefore, these findings suggest that Eq. (13) and (14) can be used to estimate K_r and τ_c well under biochar addition in this study.

The above results demonstrate that long-term biochar addition effectively changed soil properties, resulting in reduction of K_r and increase of τ_c across all biochar treatments compared to the control. The reduction of K_r and increase of τ_c had a positive relationship with both rates and durations of biochar addition, with the rate exerting a stronger influence than the duration. The MWD and COH were identified as the main factors that influenced K_r and τ_c, thus were used to predict K_r and τ_c in 2018 and 2019. In 2020, TOC, MWD, COH were used to predict K_r and τ_c under biochar addition conditions in the Loess Plateau of China.

4. Discussion

4.1. Effect of biochar addition on soil resistance

Biochar has received substantial research attention as a potential soil amendment in the last two decades. During this time, many studies have shown that it can change soil properties (Chen et al., 2020; Li et al., 2023; Zhang et al., 2021), and thus may impact soil resistance (K_r and τ_c) (Gholamahmadi et al., 2023; Li et al., 2024). This study in China's Loess Plateau has shown that biochar addition generally reduced rill erodibility (K_r) by 30 % but lightly increased critical shear stress (τ_c) (1 %) on average across the study years compared to bare soil (Table 4), which shows that biochar enhanced the ability of soil to resistance detachment by the concentrated water flow. This result is consistent with the findings of Seitz et al. (2020), who observed a decrease of soil erodibility in sandy and silty soils with the addition of biochar. Moreover, Parhizkar et al. (2023) also found biochar addition decreased K_r by 79 % compared to the control. The reason for the K_r reduction and τ_c increase might be that biochar is characterized by a high level of porosity, high specific surface area, and high cation exchange capacity (CEC) (de Sousa Lima et al., 2018; Xu et al., 2019). As a result, biochar has high adsorption

capacity and interacts with soil ions, organic matter, and clay, thus biochar addition, as soil amendment, improves soil aggregate stability and increases soil COH (Table 3), which might enhance resistance of soil mass to detachment by water flow. Moreover, biochar, being rich in carbon, contributes to high TC and TOC. This fosters the bonding of soil particles, leading to increased aggregate formation and enhancement of soil stability, which thus also increases soil's resistance to erosion by flowing water, leading to a reduction of K_r and an increase of τ_c. This study showed that biochar addition elevated soil COH, MWD, TC and TOC, and these chemical and physical properties exhibited negative correlations with K_r but positive correlations with τ_c (Fig. 3), consequently, biochar addition greatly decreased K_r but increased τ_c. The above results reflect the elevation of soil resistance to water erosion due to biochar addition on loessial slopes.

4.2. Variation of soil resistance with biochar addition rate

The impact of biochar addition on K_r and τ_c depended on the biochar addition rate, with a moderate addition rate having the potential to enhance soil resistance. Biochar addition at low rates (1 %, 2.5 % or 4 %, w/w) generally decreased K_r but increased τ_c, Conversely, 5.5 % and 7 % biochar addition significantly increased K_r and reduced τ_c relative to the control after short-term biochar addition (2018 and 2019). Our findings align with those of Li et al. (2019), who found that 1 % and 3 % biochar addition decreased runoff and inhibited soil loss, while the opposite effect was observed at higher addition rates (5 and 7 %) under simulated rainfall. Similarly, Cai et al. (2020) observed that biochar addition at a 5 % rate effectively decreased both runoff and soil loss, but 7 % addition promoted soil loss. The reason might be that biochar addition with higher rates and short-term duration increased soil looseness, subsequently weakening the resistance of soil to erosion. However, the outcomes from previous studies diverge from our observations, indicating a substantial reduction in soil loss with escalating biochar addition rates in short-term simulated experiments (Abrol et al., 2016; Jien and Wang, 2013; Nyambo et al., 2018; Vahidi et al., 2022; Zeng et al., 2014). We hypothesize that these contradictory effects might stem from variations in soil composition between our study and prior research. Previous studies primarily featured soils composed mainly of clay and silt particles (Jien and Wang, 2013; Zeng et al., 2014). A higher clay content, characterized by a large specific surface area, facilitates the interaction between soil and biochar. This interaction can result in soil particles binding more tightly, either directly with biochar or initially adsorbing soil organic matter and subsequently binding to adjacent soil particles. This behavior leads to the incorporation of biochar into aggregates, thereby bolstering aggregate stability (Yang and Lu, 2021). As a consequence, soil erosion diminishes with higher rates of biochar application. Nevertheless, our study revealed that the soil predominantly consisted of sand and silt particles. The adsorption capacity of coarse soil particles, such as sand, for biochar and other soil particles was weaker compared to that of finer soil particles like clay. Consequently, treatments with elevated biochar addition rates did not yield statistically significant differences in water-stable soil aggregate content in 2018 and 2019 (Table 3). Furthermore, our findings indicate a negative correlation between the biochar addition rate and soil resistance under short-term biochar addition.

4.3. Temporal effects of biochar addition duration on soil resistance

Long-term biochar addition (2020) reduced K_r and increased τ_c regardless of addition rates, and the effect was proportional to the biochar addition durations (Table 4). Biochar significantly influenced MWD, COH, BD, TC and TOC then K_r and τ_c (Fig. 3). However, only MWD, COH and BD correlated with K_r and τ_c in 2018 and 2019 (Fig. 5). The limited correlation between K_r, τ_c and TOC could be attributed to the fact that the enhancement of soil structure due to TOC from biochar occurs gradually. Both the high TOC and adsorption capacity of biochar played a role in binding soil particles and forming new aggregates (Kang et al., 2022; Yan et al., 2022). The low correlation between K_r, τ_c and TOC, along with the significant relationship between K_r, τ_c, MWD, COH and BD, indicates most of the TOC form biochar was less available for microbial degradation in the short term due to its highly aromatic nature (Liu et al., 2022). The improvement of soil structure due to biochar addition is a gradual process that requires substantial changes in soil environments, including moisture, temperature, microbial activities, and cultivation practices. Therefore, indoor studies with relatively short durations (less than 2 years) may not adequately capture the complex dynamics of K_r and τ_c that occur under natural field conditions (Ahmadi et al., 2020; Gholami et al., 2019; Shen et al., 2021a, 2021b). Consequently, the adsorption capacity of biochar in this study became the main force elevating MWD and COH compared to TOC in the initial stages of biochar addition.

After biochar addition for 3 years (2020), a significant correlation between soil resistance to erosion (K_r and τ_c) and soil carbon (TC and TOC) was observed (Fig. 5). The likely reason for this was that some of the TOC from biochar might have decomposed and produced humic substances that contributed to binding soil particles to form soil aggregates and increase soil COH (Aller et al., 2017; Edeh et al., 2020; Zhang et al., 2022). Thus, the effect of TOC from biochar on K_r and τ_c started to be significant in 2020, the final year of the study. Besides, the increase of K_r due to high biochar addition (5 % and 7 %) in 2018 and 2019, as well as 7 % biochar application in 2020 obtained the highest effect on reducing K_r and increasing τ_c implying that the adsorption capacity of biochar from a highly specific surface area of biochar was weaker than that of humic substances and labile soil organic carbon from biochar decomposition under long-term biochar addition. The results suggest that the impact of biochar addition on soil resistance to erosion may take time to manifest and long-term biochar addition would be more beneficial to elevate soil resistance to erosion. Our results align with previous studies, demonstrating that the duration of biochar addition significantly affected soil erosion (Agbede and Adekiya, 2020; Nyambo et al., 2018). Most studies with short incubation periods reported inconsistent effects of biochar on soil erosion (positive and negative) (Cai et al., 2020; Li et al., 2019). However, results from long-term field experiments consistently showed a reduction of soil loss and runoff following biochar addition (Gholamahmadi et al., 2023; Li et al., 2024; Vahidi et al., 2022).

4.4. Soil resistance estimation and limitations

Multivariate nonlinear regression analysis identified that MWD and COH were the main factors useful for simulating K_r and τ_c in 2018 and 2019. Notably, TOC also became significant factor in the models in 2020. TOC was excluded during the analysis process in 2018 and 2019, probably because TOC from biochar was ineffective for enhancing soil structure in the early years. Biochar is known to be rich in carbon, but much of the carbon is inert (Adhikari et al., 2024; Luo et al., 2023). Consequently, the estimation of K_r and τ_c under biochar addition was complicated and inconsistent with some previous studies (Elliot and Flanagan, 2023; Ostovari et al., 2022). The results confirmed that the TOC from biochar could be used to estimate K_r and τ_c in the case of long-term biochar addition. Consequently, power regression models were formulated and effectively estimated the K_r and τ_c across all biochar treatments, encompassing both short-term and long-term biochar additions. Actually, the K_r, representing the slope of the equation that interpolates rill detachment capacity and shear stress, serves as a quantifiable measure of a soil's resistance to rill erosion (Nearing et al., 1991). Hence, the accurate estimation of K_r is essential for the implementation of effective soil conservation measures.

The K_r decrease and τ_c increase observed in sites treated with biochar, in comparison to untreated soils, can help us to comprehensively understand the hydrological consequences of biochar addition, including its dynamic and variable influences on soil properties,

erodibility and soil loss under the long-term field experiments with continuous monitoring. This finding provides valuable insights into the complex interactions between biochar, soil erosion processes, and environmental factors, improving our understanding of the efficacy and potential risks associated with biochar application in soil erosion management. This knowledge could inform improvements to soil conservation programs aimed at mitigating soil erosion risks. Notably, our study provides recommendations for optimal models to mitigate K_r and τ_c under different rates and durations of biochar addition. Moreover, the establishment of models for predicting K_r and τ_c will be helpful to estimate K_r and τ_c, and can support soil erosion models when there isn't sufficient data about the effects of biochar amendment.

However, there is a potential limitation of a few soil properties considered here, combined with a simulated flow scour test. Therefore, it is imperative to conduct further flow scour tests in various field settings, considering a broader range of soil properties, to enhance the reliability and applicability of the results obtained in this study. Additionally, the effect of biochar addition on soil properties varied with experiment conditions, such as soil texture, management conditions (e.g., cropping systems, irrigation methods) (Faloye et al., 2024; Kang et al., 2022; Li et al., 2024; Wang et al., 2019), biochar types and production temperature (Ghorbani and Amirahmadi, 2024), thus the results and empirical equations obtained from our study were regraded to apple branch biochar (OR woody material) and pyrolysis temperature of 550 °C, and should undergo calibration to estimate K_r and τ_c in more experimental conditions. Despite these acknowledged limitations, this study effectively delineated the impact of biochar on K_r and τ_c, and devised distinct models for predicting K_r and τ_c based on various soil properties. This guidance also holds significant importance for the judicious application of biochar in soil erosion management and efforts toward soil restoration on the Loess Plateau.

5. Conclusions

Biochar can play a crucial role in soil erosion processes by increasing soil's resistance to erosion, and thus far, this aspect has not been systematically explored. This study was carried out to investigate the effect of biochar addition rate and duration on K_r and τ_c through a flume experiment, explore the key factors influencing the temporal variation in K_r and τ_c, and model soil resistance to erosion under biochar addition. The results demonstrate that across years and rates, biochar decreased K_r, while increasing τ_c. Notably, the K_r reduction and τ_c elevation were observed at lower rates of biochar addition, rather than at high rates, after biochar addition for 1 and 2 years. Contrastingly, K_r decreased, while τ_c increased proportionally with the escalating biochar addition rates over the 3-year biochar addition. The results indicate that the greater effect of biochar addition on K_r and τ_c was observed with higher rates and long-term biochar addition. Soil consolidation, structural stability, soil organic matter, and the mean weight diameter of soil aggregates (MWD) negatively are related with the alterations K_r, but positively related with τ_c. Thus, soil cohesion, MWD, and total organic carbon (TOC) were used to accurately estimated K_r and τ_c under biochar addition (R^2=0.761).

Exploring the effect of biochar on the mechanism of K_r and τ_c contributes to explaining the effects of biochar on soil detachment and soil erosion processes. Our study provides insights how long-term biochar addition enhances soil's potential resistance to detachment and erosion. The established fitted equations for predicting K_r and τ_c could help identify which soil properties vary with biochar addition and is valuable for supporting soil erosion modeling when data about biochar amendments are insufficient. However, this study just considered the effects of one type of biochar on K_r and τ_c for one soil type and limited soil properties that could influence the rill erosion process. As a result, designing novel experiments which consider more soil properties are necessary to broadly understand the long-term effects of different biochar types on diverse soil erosion susceptibilities.

Declaration of Competing Interest

The authors declare that they have no known competing financial interests or personal relationships that could have appeared to influence the work reported in this paper.

Data Availability

Data will be made available on request.

Acknowledgements

This work was supported by the National Natural Science Foundation of China (No. 42177338, 42207381 and 42361144707), the China Postdoctoral Science Foundation (2023M733230), the Fundamental Research Funds for the Central Universities (2023HHZX001), the Soft Science Research Project of Henan Province (242400410184), and the open project of State Key Laboratory of Soil Erosion and Dryland Farming on the Loess Plateau, Northwest A&F University (No. F2010121002–202418).

References

Abrol, V., Ben-Hur, M., Verheijen, F.G.A., Keizer, J.J., Martins, M.A.S., Tenaw, H., Tchehansky, L., Graber, E.R., 2016. Biochar effects on soil water infiltration and erosion under seal formation conditions: rainfall simulation experiment. Sci. Total Environ. 16, 2709–2719. https://doi.org/10.1007/s11368-016-1448-8.

Adhikari, S., Moon, E., Paz-Ferreiro, J., Timms, W., 2024. Comparative analysis of biochar carbon stability methods and implications for carbon credits. Sci. Total Environ. 914, 169607. https://doi.org/10.1016/j.scitotenv.2023.169607.

Agbede, T.M., Adekiya, A.O., 2020. Influence of biochar on boil physicochemical properties, erosion potential, and maize (Zea mays L.) grain yield under sandy soil condition. Commun. Soil Sci. Plan, 51, 2559–2568. https://doi.org/10.1080/00103624.2020.1845348.

Ahmadi, S.H., Ghasemi, H., Sepaskhah, A.R., 2020. Rice husk biochar influences runoff features, soil loss, and hydrological behavior of a loamy soil in a series of successive simulated rainfall events. Catena 192, 104587. https://doi.org/10.1016/j.catena.2020.104587.

Aller, D., Mazur, R., Moore, K., Hintz, R., Laird, D., Horton, R., 2017. Biochar age and crop rotation impacts on soil quality. Soil Sci. Soc. Am. J. 81, 1157–1167. https://doi.org/10.2136/sssaj2017.01.0010.

Al-Madhhachi, A.T., Hanson, G.J., Fox, G.A., Bockenstedt, P.J., Bulut, R., 2013. Determining erodibility parameters of undisturbed soil using a laboratory jet erosion test. Trans. ASABE 56, 489–504. https://doi.org/10.13031/trans.56.9838.

An, S.S., Darboux, F., Cheng, M., 2013. Revegetation as an efficient means of increasing soil aggregate stability on the loess plateau (China). Geoderma 209–210, 75–85. https://doi.org/10.1016/j.ecoleng.2014.05.011.

Busscher, W.J., Novak, J.M., Evans, D.E., Watts, D.W., Niandou, M.A.S., Ahmedna, M., 2010. Influence of pecan biochar on physical properties of a norfolk loamy sand. Soil Sc. 175, 10–14. https://doi.org/10.1016/j.eja.2021.126345.

Cai, W., Huang, H., Chen, P., Huang, X., Gaurav, S., Pan, Z., Lin, P., 2020. Effects of biochar from invasive weed on soil erosion under varying compaction and slope conditions: comprehensive study using flume experiments. Biomass-.-. Convers. Biores. 2020, 1–20. https://doi.org/10.1007/s13399-020-00943-3.

Cao, L.X., Zhang, K.L., Dai, H.L., Guo, Z.L., 2011. Modeling soil detachment on unpaved road surfaces on the Loess Plateau. Trans. ASABE 54, 1377–1384. https://doi.org/10.13031/2013.39039.

Chen, X.P., Zhou, B.B., Wang, Q.J., Tao, W.H., Lin, H., 2020. Nano-biochar reduced soil erosion and nitrate loss in sloping fields on the Loess Plateau of China. Catena 187, 104346. https://doi.org/10.1016/j.catena.2019.104346.

Cochrane, T.A., Flanagan, D.C., 1997. Detachment in a simulated rill. Trans. ASAE 40, 111–119. https://doi.org/10.13031/2013.21255.

Delgado, M.I., 2018. Soil loss as a result of the interactions between natural landscape attributes and human activities in Ventania, Argentina. Ecol. ía Austral 28, 074–080. https://doi.org/10.25260/EA.18.28.1.0.608.

Ebabu, K., Taye, G., Tsunekawa, A., Haregeweyn, N., Adgo, E., Tsubo, M., et al., 2023. Land use, management and climate effects on runoff and soil loss responses in the highlands of Ethiopia. J. Environ. Manag. 326, 116707. https://doi.org/10.1016/j.jenvman.2022.116707.

Edeh, I.G., Maek, O., Buss, W., 2020. A meta-analysis on biochar's effects on soil water properties - new insights and future research challenges, 136857–136857 Sci. Total Environ. 714. https://doi.org/10.1016/j.scitotenv.2020.136857.

Elliot, W.J., Flanagan, D.C., 2023. Estimating WEPP cropland erodibility values from soil properties. J. ASABE 66, 329–351. https://doi.org/10.13031/ja.15218.

Faloye, O.T., Ajayi, E.A., Rostek, J., Schroeren, V., Babalola, T., Fashina, A., Horn, R., 2024. Hydraulic and pore functions of differently textured soils modified by biochar from different parts of the mango plant. Soil Till. Res. 236, 105944. https://doi.org/10.1016/j.still.2023.105944.

Ferreira, C.S., Seifollahi-Aghmiuni, S., Destouni, G., Ghajarnia, N., Kalantari, Z., 2022. Soil degradation in the European Mediterranean region: Processes, status and consequences. Sci. Total Environ. 805, 150106. https://doi.org/10.1016/j.scitotenv.2021.150106.

Flanagan, D.C., Nearing, M.A., 1995. USDA-Water Erosion Prediction Project (WEPP). WEPP Users Summary. NSERL Report, vol. 10. USDA-ARS National Soil Erosion Research Laboratory, West Lafayette, Indiana.

Foster, G.R., 1982. Modeling the erosion process. Hydrologic modeling of small watersheds. American Society of Agricultural Engineers, pp. 295–380. ⟨https://www.cabidigitallibrary.org/doi/full/10.5555/19851999449⟩.

Gao, Y., Shao, G., Yang, Z., Zhang, K., Lu, J., Wang, Z., Wu, S., Xu, D., 2021. Influences of soil and biochar properties and amount of biochar and fertilizer on the performance of biochar in improving plant photosynthetic rate: a meta-analysis. Eur. J. Agron. 130, 126345. https://doi.org/10.1016/j.eja.2021.126345.

Gholamahmadi, B., Jeffery, S., Gonzalez-Pelayo, O., Prats, S.A., Bastos, A.C., Keizer, J.J., Verheijen, F.G.A., 2023. Biochar impacts on runoff and soil erosion by water: A systematic global scale meta-analysis. Sci. Total Environ. 871, 161860. https://doi.org/10.1016/j.scitotenv.2023.161860.

Gholami, L., Karimi, N., Kavian, A., 2019. Soil and water conservation using biochar and various soil moisture in laboratory conditions. Catena 182, 104151. https://doi.org/10.1016/j.catena.2019.104151.

Ghorbani, M., Amirahmadi, E., 2024. Insights into soil and biochar variations and their contribution to soil aggregate status – A meta-analysis. Soil Till. Res. 244, 106282. https://doi.org/10.1016/j.still.2024.106282.

Guo, R., Qian, R., Yang, L., Khaliq, A., Han, F., Hussain, S., Zhang, P., Cai, T., Jia, Z., Chen, X., Ren, X., 2022. Interactive effects of maize straw-derived biochar and N fertilization on soil bulk density and porosity, maize productivity and nitrogen use efficiency in arid areas. J. Soil Sci. Plant Nut. 22, 4566–4586. https://doi.org/10.1007/s42729-022-00881-1.

Gyssels, G., Poesen, J., Nachtergaele, J., Govers, G.J.S., Research, T., 2002. The impact of sowing density of small grains on rill and ephemeral gully erosion in concentrated flow zones. Soil Till. Res. 64, 189–201. https://doi.org/10.1016/S0167-1987(01)00263-X.

Hao, H.X., Qin, J.H., Sun, Z.X., Guo, Z.L., Wang, J.G., 2021. Erosion-reducing effects of plant roots during concentrated flow under contrasting textured soils. Catena 203, 105378. https://doi.org/10.1016/j.catena.2021.105378.

He, X., Zhou, J., Zhang, X., Tang, K., 2006. Soil erosion response to climatic change and human activity. Reg. Environ. Chang. 6, 62–70. https://doi.org/10.1007/s10113-005-0004-7.

Huang, X., Niu, R., Huang, X., An, Y., Li, J., Li, M., Huang, H., Garg, A., 2021. Influence of sustainable biochars produced from kitchen waste, pig manure, and wood on soil erosion. Water 13, 2296. https://doi.org/10.3390/w13162296.

Jien, S.H., Wang, C.S., 2013. Effects of biochar on soil properties and erosion potential in a highly weathered soil. Catena 110, 225–233. https://doi.org/10.1016/j.catena.2013.06.021.

Kang, M.W., Yibeltal, M., Kim, Y.H., Oh, S.J., Lee, J.C., Kwon, E.E., Lee, S.S., 2022. Enhancement of soil physical properties and soil water retention with biochar-based soil amendments. Sci. Total Environ. 836, 155746. https://doi.org/10.1016/j.scitotenv.2022.155746.

Klute, A., Kemper, W.D., Rosenau, R.C., 1986. Aggregate stability and size distribution. Soil Science Society of America. In: SSSA Book Series. American Society of Agronomy.

Lei, T.W., Zhang, Q.W., Zhao, J., Xia, W.S., 2002. Soil detachment rates for sediment loaded flow in rills. Trans. ASAE. 45, 1897–1903. https://doi.org/10.13031/2013.11440.

Li, Y., Feng, G., Tewolde, H., 2023. Biochar derived from papermill factories improves soil physical and hydraulic properties in no-till cotton fields. Biochar 5, 1–18. https://doi.org/10.1007/s42773-023-00235-9.

Li, Y., Yang, J., Yang, M., Zhang, F., 2024. Exploring biochar addition impacts on soil erosion under natural rainfall: A study based on four years of field observations on the Loess Plateau. Soil Till. Res. 236, 105935. https://doi.org/10.1016/j.still.2023.105935.

Li, Y.Y., Zhang, F.B., Yang, M.Y., Zhang, J.Q., Xie, Y.G., 2019. Impacts of biochar application rates and particle sizes on runoff and soil loss in small cultivated loess plots under simulated rainfall. Sci. Total Environ. 649, 1403–1413. https://doi.org/10.1016/j.scitotenv.2018.08.415.

Liang, J., Li, Y., Si, B., Wang, Y., Chen, X., Wang, X., Chen, H., Wang, H., Zhang, F., Bai, Y., Biswas, A., 2021. Optimizing biochar application to improve soil physical and hydraulic properties in saline-alkali soils. Sci. Total Environ. 771, 144802. https://doi.org/10.1016/j.scitotenv.2020.144802.

Liu, H., Wang, X., Song, X., Leng, P., Li, J., Rodrigues, J.L.M., et al., 2022. Generalists and specialists decomposing labile and aromatic biochar compounds and sequestering carbon in soil. Geoderma 428, 116176. https://doi.org/10.1016/j.geoderma.2022.116176.

Liu, J.X., Liu, G.B., Flanagan, D.C., Wang, B., Wang, Z.Y., Xiao, J., 2020. Effects of soil-incorporated plant litter morphological characteristics on the soil detachment process in grassland on the loess plateau of China. Sci. Total Environ. 705, 134651. https://doi.org/10.1016/j.scitotenv.2019.134651.

Liu, J.X., Chen, L.D., Wang, B., Peng, X.Y., 2024. Effects of physical crust on soil detachment by overland flow in the Loess Plateau region of China. Int. Soil Water Conse 12, 107–120. https://doi.org/10.1016/j.iswcr.2023.05.006.

Luk, S.H., Merz, W., 1992. Use of the slat tracing technique to determine the velocity of overland flow. Soil Tech. 5, 289–301 http://pascal-francis.inist.fr/vibad/index.php?action=getRecordDetail&idt=4680685.

Luo, L., Wang, J.X., Lv, J.T., Liu, Z.G., Sun, T.R., Yang, Y., Zhu, Y.G., 2023. Carbon sequestration strategies in soil using biochar: advances, challenges, and opportunities. Environ. Sci. Technol. 57, 11357–11372. https://doi.org/10.1021/acs.est.3c02620.

2023. Maisyarah, S., Chen, J.Y., Hseu, Z.Y., Jien, S.H., 2023. Retention and loss pathways of soluble nutrients in biochar-treated slope land soil based on a rainfall simulator. S. E. H. 1, 100021. https://doi.org/10.1016/j.seh.2023.100021..

Meinen, B.U., Robinson, D.T., 2021. Agricultural erosion modelling: evaluating USLE and WEPP field-scale erosion estimates using UAV time-series data. Environ. Modell. Softw. 137, 104962. https://doi.org/10.1016/j.envsoft.2021.104962.

Nearing, M.A., Bradford, J.M., Parker, S., 1991. Soil detachment by shallow flow at low slopes. Soil Sci. Soc. Am. J. 55, 351–357. https://doi.org/10.2136/sssaj1991.03615995005500020006x.

Niu, Y., Gao, Z., Li, Y., Lou, Y., Zhang, S., Zhang, L., Du, J., Zhang, X., Luo, K., 2020. Characteristics of rill erosion in spoil heaps under simulated inflow: A field runoff plot experiment. Soil Till. Res. 202, 104655. https://doi.org/10.1016/j.still.2020.104655.

Nyambo, P., Taeni, T., Chiduza, C., Araya, T., 2018. Effects of maize residue biochar amendments on soil properties and soil loss on acidic hutton soil. Agronomy 8, 256. https://doi.org/10.3390/agronomy8110256.

Ostovari, Y., Moosavi, A.A., Mozaffari, H., Poppiel, R.R., Tayebi, M., Demattê, J.A., 2022. Soil erodibility and its influential factors in the Middle East. In Computers in Earth and Environmental Sciences. Elsevier, pp. 441–454.

Parhizkar, M., Shabanpour, M., Lucas-Borja, M.E., Zema, D.A., Li, S., Tanaka, N., Cerda, A., 2021. Effects of length and application rate of rice straw mulch on surface runoff and soil loss under laboratory simulated rainfall. Int. J. Sediment Res 36, 468–478. https://doi.org/10.1016/j.ecoleng.2023.106964.

Parhizkar, M., Shabanpour, M., Lucas-Borja, M.E., Zema, D.A., 2023. Effects of rice husk biochar on rill detachment capacity in deforested hillslopes. Ecol. Eng. 191, 106964. https://doi.org/10.1016/j.ecoleng.2023.106964.

Sadeghi, S.H.R., Moosavi, V., Karami, A., Behnia, N., 2012. Soil erosion assessment and prioritization of affecting factors at plot scale using the Taguchi method. J. Hydrol. 448, 174–180. https://doi.org/10.1016/j.jhydrol.2012.04.038.

Seitz, S., Teuber, S., Geiler, C., Goebes, P., Scholten, T.J.S.S., 2020. How do newly-amended biochar particles affect erodibility and soil water movement?—a small-scale experimental approach. Soil Syst. 4, 1–14. https://doi.org/10.3390/soilsystems4040060.

Shen, N., Wang, Z., Guo, Q., Zhang, Q., Zhang, F., 2021a. Soil detachment capacity by rill flow for five typical loess soils on the loess plateau of China. Soil Till. Res. 213, 105159. https://doi.org/10.1016/j.still.2021.105159.

Shen, Z., Zhang, Z., Zhang, M., Rinklebe, J., Ma, Y., Hou, D., 2021b. Effect of production temperature and particle size of rice husk biochar on mercury immobilization and erosion prevention of a mercury contaminated soil. J. Hazard. Mater. 420, 126646. https://doi.org/10.1016/j.jhazmat.2021.126646.

Shi, G., Wu, Y., Li, T., Fu, Q., Wei, Y., 2022b. Mid- and long-term effects of biochar on soil improvement and soil erosion control of sloping farmland in a black soil region, China. J. Environ. Manag. 320, 115902. https://doi.org/10.1016/j.jenvman.2022.115902.

Shi, H.Q., Xiao, H., Liu, G., Abd Elbasit, M.A., Zheng, F., Zhang, Q., Zhang, Y., Guo, Z., 2022a. Identifying interrill, rill, and ephemeral gully erosion evolution by using rare earth elements as tracers. J. Hydrol. 612, 128271. https://doi.org/10.1016/j.jhydrol.2022.128271.

Situ, G., Zhao, Y., Zhang, L., Yang, X., Chen, D., Li, S., Wu, Q., Xu, Q., Chen, J., Qin, H., 2022. Linking the chemical nature of soil organic carbon and biological binding agent in aggregates to soil aggregate stability following biochar amendment in a rice paddy. Sci. Total Environ. 847, 157460. https://doi.org/10.1016/j.scitotenv.2022.157460.

de Sousa Lima, J.R., Silva, Wd.M., de Medeiros, E.V., Duda, G.P., Correa, M.M., Martins Filho, A.P., Clermont-Dauphin, C., Dantas Antonino, A.C., Hammecker, C., 2018. Effect of biochar on physicochemical properties of a sandy soil and maize growth in a greenhouse experiment. Geoderma 319, 14–23. https://doi.org/10.1016/j.geoderma.2017.12.033.

Tang, X., Miao, C., Xi, Y., Duan, Q., Lei, X., Li, H., 2018. Analysis of precipitation characteristics on the loess plateau between 1965 and 2014, based on high-density gauge observations. Atmos. Res. 213, 264–274. https://doi.org/10.1016/j.atmosres.2018.06.013.

Vahidi, M.J., Zahan, M.H.S., Atajan, F.A., Parsa, Z., 2022. The effect of biochars produced from barberry and jujube on erosion, nutrient, and properties of soil in laboratory conditions. Soil Till. Res. 219, 105345. https://doi.org/10.1016/j.still.2022.105345.

Wang, B., Zhang, G.H., Yang, Y.F., Li, P.P., Liu, J.X., 2018. The effects of varied soil properties induced by natural grassland succession on the process of soil detachment. Catena 166, 192–199. https://doi.org/10.1016/j.catena.2018.04.007.

Wang, D., Li, C., Parikh, S.J., Scow, K.M., 2019. Impact of biochar on water retention of two agricultural soils–a multi-scale analysis. Geoderma 340, 185–191. https://doi.org/10.1016/j.geoderma.2019.01.012.

Wang, H., Zhang, G.H., 2021. Temporal variation in soil erodibility indices for five typical land use types on the Loess Plateau of China. Geoderma 381, 114695. https://doi.org/10.1016/j.geoderma.2020.114695.

Xu, D., Cao, J., Li, Y., Howard, A., Yu, K., 2019. Effect of pyrolysis temperature on characteristics of biochars derived from different feedstocks: A case study on ammonium adsorption capacity. Waste Manag. 87, 652–660. https://doi.org/10.1016/j.wasman.2019.02.049.

Yan, M., Li, X., Liu, Y., Li, Y., He, L., Zhang, J., 2022. Biochar enhanced soil aggregation and c-related enzyme activity in post-mining land on the loess plateau, China. Land Degrad. Dev. 33, 1054–1061. https://doi.org/10.1002/ldr.4230.

Yang, C.D., Lu, S.G., 2021. Effects of five different biochars on aggregation, water retention and mechanical properties of paddy soil: A field experiment of three-season crops. Soil Till. Res. 205, 104798. https://doi.org/10.1016/j.still.2020.104798.

Yin, X.A., Zhao, L.S., Fang, Q., Zi, R.Y., Fang, F.Y., Yang, X.C., Ding, G.J., 2024. Effects of biochar amendment on the surface and underground runoff and soil loss of karst slopes at the microplot scale. Catena 238, 107857. https://doi.org/10.1016/j.catena.2024.107857.

Zeng, Y.H., Shih, H.J., Wei, H.C., Ruei, C.L., 2014. Impacts of biochar on physical properties and erosion potential of a mudstone slopeland soil. Sci. World Jo 2014, 602197. https://doi.org/10.1155/2014/602197.

Zhang, F.B., Huang, C.H., Yang, M.Y., Zhang, J.Q., Shi, W.Y., 2019. Rainfall simulation experiments indicate that biochar additionenhances erosion of loess-derived soils. Land Degrad. Dev. 30, 2272–2286. https://doi.org/10.1002/ldr.3399.

Zhang, G., Dou, S., Meng, F.R., Yin, X.B., Zhou, X., 2022. Transformation of biochar into extracted humic substances under short-term laboratory incubation conditions: evidence from stable carbon isotopes. Soil Till. Res. 215, 105189. https://doi.org/10.1016/j.still.2021.105189.

Zhang, G.H., 2002. Experimental simulation on effect of scouring time on soil detachment rate. J. Soil Water Conserv. (Chin. Abstr.) 16, 1–4. ⟨http://stbcxb.cnjournals.com/stbcxben/article/abstract/20020276⟩.

Zhang, G.H., Liu, B.Y., Liu, G.B., He, X.W., Nearing, M.A., 2003. Detachment of undisturbed soil by shallow flow. Soil Sci. Soc. Am. J. 67, 713–719. https://doi.org/10.2136/sssaj2003.7130.

Zhang, G.H., Ding, W.F., Jian, P.U., Li, J.M., Qian, F., Sun, B.Y., 2020. Effects of moss-dominated biocrusts on soil detachment by overland flow in the Three Gorges Reservoir Area of China. J. Mt. Sci. -Engl. 17, 2418–2431. https://doi.org/10.1007/s11629-020-6200-6.

Zhang, M., Yu, S., Ye, Q., Li, Z., Yin, D., Zhao, Z., 2023. Effect of the grain-for-green program on forest fragmentation. Land Degrad. Dev. 34, 3208–3224. https://doi.org/10.1002/ldr.4678.

Zhang, Y., Wang, J., Feng, Y., 2021. The effects of biochar addition on soil physicochemical properties: a review. Catena 202, 105284. https://doi.org/10.1016/j.catena.2021.105284.